Magnetization Excitation in FeMn Antiferromagnetic Film by Injection of Spins With Current in Thin-Film THz Emitters Structures

A. Panas[1], E. Vilkov[2], S. Chigarev[2], and O. Byshevski-Konopko[2]

[1]A.I. Shokin ISTOK Research and Production Enterprise, 141190 Fryazino, Russia
[2]Kotel'nikov Institute of Radio Engineering and Electronics (Fryazino Branch), Russian Academy of Sciences, 141190 Fryazino, Russia

This article is devoted to the study of the possibility of excitation of the intrinsic magnetization in the FeMn antiferromagnetic (AFM) film by injecting spins into it with a relatively low current. Such a possibility is shown on the basis of the operation of spin injection THz sources using this effect. It has been shown that the use of this effect in THz spin-injection emitters is of interest both from the point of view of developing theoretical ideas about the magnetic properties of AFMs and from a practical point of view of the use of these sources. New experimental results have been obtained, developing theoretical ideas about the intrinsic magnetization of thin films of AFMs.

Index Terms— **Intrinsic magnetization, metallic antiferromagnetic (AFM), spin-polarized current, terahertz radiation.**

I. Introduction

IN RECENT years, much attention has been paid to the study of the possibility of intrinsic magnetization excitation in thin antiferromagnetic (AFM) films. This is due to the fact that AFM films are resistant to disturbances caused by external magnetic fields, do not generate scattered fields, and, at the same time, demonstrate ultra-fast dynamics [1]. One of the directions of their practical application, in addition to information technologies, can be the construction of a new generation of solid-state small-size sources of electromagnetic oscillations in the THz range (1–30 THz) [1]–[3]. This possibility is related to the fact that the magnetization, induced by spin-polarized current in magnetic transitions [4] with AFM, determines the exchange splitting of conduction electrons in them. As a result, the radiation frequency given by the exchange splitting [5] in AFM film emitters will depend on current (its density) and can change with the change of current. In addition, the operating current in emitters with AFM films can be significantly lower than in film emitters with ferromagnetic (FM) films. It is also attractive that the use of AFM films in these THz emitters increases their resistance to external magnetic fields. In general, the observation of THz radiation during current flow in thin-film structures, including AFM films, can serve as a test of intrinsic magnetization excitation in them and be used as a tool to study this effect.

In the study of thin-film contacts consisting of layers of FM–AFM, much attention is paid to processes based on spin-orbit interaction in magnetic nanojunctions through which the electric current flows. Thus, in [6] and [7], a layered thin-film Pt-AFM structure with an electric conduction current in a platinum layer was studied. The authors paid attention to the bevel and rotation of the AFM sublattices under the action of a spin current that arises in the platinum layer due to spin-orbit scattering of conduction electrons. They showed that, in this structure, radiation generation in the range of 0.5–2 THz is possible due to the irregular rotation of the AFM sublattices resulting from the crystal anisotropy of the AFM.

Another approach to the creation of solid-state THz emitters with magnetic thin-film structures is based on the use of the sd-exchange interaction mechanism, which was first described in [5]–[8]. In this case, when a spin-polarized electron flow crosses the interface of two FMs with different magnetic properties, in general, two processes of changing the spin state of the electrons are observed. The first, the torsion mechanism or the Slonczewski–Berger mechanism, is associated with the transfer of the transverse component of the spin, oriented along with the magnetization of the first layer, into the lattice of the second FM. As a result, the spins acquire a direction parallel or antiparallel with respect to the magnetization of the second layer, occupying, respectively, levels in the spin-energy subbands. This process is observed at a distance of several nanometers. Since the energy of electrons changes faster than their spin state, spin-unbalanced, energetically excited electrons appear in the subbands, which carry out spin-flip transitions between the subbands with the emission of an energy quantum. This second process of uncompensated spin transfer is observed at a distance of tens of nanometers. It leads to spin-flip transitions and is called spin current injection in magnetic transitions.

In [9]–[15], both theoretically and experimentally, the influence of the current flowing through magnetic FM–AFM junction on the structure of the AFM layer was investigated. The practical significance of sd-exchange interaction was confirmed in subsequent works [16]–[19], where the generation of THz radiation was explained by the injection of spins with the current in magnetic junctions. Injection of spins by the

Manuscript received April 23, 2021; accepted February 5, 2022. Date of publication February 10, 2022; date of current version March 18, 2022. Corresponding author: A. Panas (e-mail: aipanas@istokmw.ru).

Color versions of one or more figures in this article are available at https://doi.org/10.1109/TMAG.2022.3150892.

Digital Object Identifier 10.1109/TMAG.2022.3150892

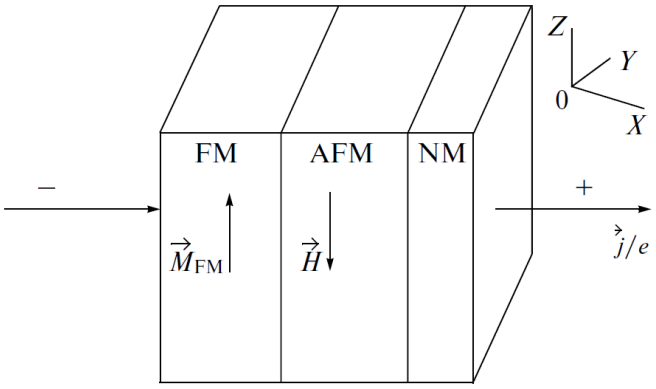

Fig. 1. Scheme of the calculated FM–AFM structure: $\mathbf{M}_{\mathrm{FM}}$ is the magnetization of the FM layer and $\mathbf{j}/e$ is the flux density of conduction electrons in the layers.

current was first considered in [20]. This field of research has been developed in [21]–[23], where, depending on the materials of the magnetic junction layers used, radiation in the frequency range of 7–30 THz at operating currents of up to several hundred mA was experimentally observed.

In [24] and [25], the possibility of intrinsic magnetization in the AFM layer due to the beveling of its sublattices with spins injected from the FM layer with a current of tens of mA was predicted. In terms of creating spin injection THz range emitters, the use of the AFM layer in magnetic nanojunctions is quite attractive. It can reduce the operating current and provide additional control over the frequency response of the emitted signal. Despite the fact that this effect was experimentally confirmed in [26], so far, it has not been sufficiently investigated. Therefore, the purpose of this article is to expand the understanding of the intrinsic magnetization of the AFM layer arising under the action of a spin-polarized current based on a study of the operation of spin-injection emitters of the THz range using AFM layers. As an experimental tool to prove this, the authors use the THz radiation that they observe during the passage of current in the magnetic junction. Such radiation, which has a non-thermal nature, according to the authors, is possible only when magnetism appears in the second junction layer. Therefore, the research focuses on proving the non-thermal nature of this radiation. In addition, in this work, the authors show the practical importance of the emitters under study.

II. Theoretical Concepts of Intrinsic Magnetization Occurrence in AFM Under the Action of Spin-Polarized Current

A typical scheme of the investigated transition is shown in Fig. 1. The FM layer is considered to be quite rigid—the spins of the electrons and the lattice are fixed. In this structure, this layer plays the role of an injector. The AFM layer is a metal with free electron spins and magnetization. This layer acts as a "working layer" or collector. It collects electrons injected by the current, and the spin equilibrium is violated. The collector is followed by a layer of normal metal NM, which serves to close the electrical circuit. Between these three layers, ultra-thin "buffer" matching layers can be placed. One of the purposes of their introduction is to prevent direct exchange interaction of lattices so that the connection between the FM, AFM, and NM layers is determined only by the electric current passing through them. Let us consider the process of the appearance of induced magnetization in the AFM layer of the FM–AFM magnetic transition due to beveling of its magnetic sublattices (departure from the antiparallel direction of the magnetization of the sublattices leads to the appearance of an angle between them), under the action of the spins injected by the current from the FM layer, based on the solution of the equation of motion of the sublattices taking into account attenuation [4]. Let us give the form of the basic transformed equations of motion for the transition AFM layer based on the "macrospin" model. In the derivation, we took into account the boundary conditions—the conditions for the continuity of spin fluxes at the section boundaries (for details, see review [4]). The equation for the precession of the total magnetization $\mathbf{M} = \mathbf{M}_1 + \mathbf{M}_2$, where $\mathbf{M}_1$ and $\mathbf{M}_2$ are the magnetizations of the sublattices, has the form

$$\begin{aligned}\frac{\partial \mathbf{M}}{\partial t} - \frac{1}{2}\frac{\kappa}{M_0}\left\{\left[\mathbf{M}\times\frac{\partial \mathbf{M}}{\partial t}\right]+\left[\mathbf{L}\times\frac{\partial \mathbf{L}}{\partial t}\right]\right\} + \gamma\,[\mathbf{M}\times\mathbf{H}] \\ + \gamma\,[\mathbf{M}\times\mathbf{H}_D] + \frac{1}{2}\gamma\left(\beta+\beta'\right)(\mathbf{M}\cdot\mathbf{n})[\mathbf{M}\times\mathbf{n}] \\ + \frac{1}{2}\gamma\left(\beta-\beta'\right)(\mathbf{L}\cdot\mathbf{n})[\mathbf{L}\times\mathbf{n}] \\ + K\left[\mathbf{M}\times\left[\mathbf{M}\times\hat{\mathbf{M}}_F\right]\right] + P_{\mathrm{sd}}\left[\mathbf{M}\times\hat{\mathbf{M}}_F\right] = 0 \end{aligned} \tag{1}$$

where $\mathbf{H}_d = -4\pi\{M_{1x}+M_{2x},0,0\}$ is the demagnetizing field, $\mathbf{n}$ is the unit vector along the anisotropy axis (the direction of this vector lies along the plane of the layers of thin films), β and β' are the anisotropy constants of AFM sublattices, M_0 is the magnetization modulus of a single sublattice, $\kappa \sim 10^{-2}$ is the Hilbert damping coefficient parameter, and γ is the gyromagnetic ratio. In (1), the current-dependent parameters arise

$$K = \frac{\mu_B Q}{eL_{\mathrm{AFM}}M_0^2}j \quad \text{and} \quad P_{\mathrm{sd}} = \frac{\gamma\,\alpha_{\mathrm{sd}}\mu_B\tau Q}{eL_{\mathrm{AFM}}}j \tag{2}$$

where j is the current density, τ is the spin relaxation time, μ_B is the Bohr magneton, $Q = (\sigma_\downarrow - \sigma_\uparrow)/\sigma$ is the degree of spin polarization of conductivity, $\sigma_{\downarrow\uparrow}$ and σ are the partial and total conductivities, e is the electron charge, L_{AFM} is the length of the AFM layer, and $\alpha_{\mathrm{sd}} \sim (2 \div 6)\cdot 10^4$ is the dimensionless sd exchange constant.

The equation of motion for the antiferromagnetism vector $\mathbf{L} = \mathbf{M}_1 - \mathbf{M}_2$ has the form

$$\begin{aligned}\frac{\partial \mathbf{L}}{\partial t} - \frac{1}{2}\frac{\kappa}{M_0}\left\{\left[\mathbf{L}\times\frac{\partial \mathbf{M}}{\partial t}\right]+\left[\mathbf{M}\times\frac{\partial \mathbf{L}}{\partial t}\right]\right\} - \gamma\,\Lambda[\mathbf{L}\times\mathbf{M}] \\ + \gamma\,[\mathbf{L}\times\mathbf{H}] + \gamma\,[\mathbf{L}\times\mathbf{H}_D] + \frac{1}{2}\gamma\left(\beta+\beta'\right)(\mathbf{M}\cdot\mathbf{n})[\mathbf{L}\times\mathbf{n}] \\ + \frac{1}{2}\gamma\left(\beta-\beta'\right)(\mathbf{M}\cdot\mathbf{n})[\mathbf{M}\times\mathbf{n}] + K\left[\mathbf{L}\times\left[\mathbf{M}\times\hat{\mathbf{M}}_F\right]\right] \\ + P_{\mathrm{sd}}\left[\mathbf{L}\times\hat{\mathbf{M}}_F\right] = 0. \end{aligned} \tag{3}$$

The uniform exchange constant Λ [27] also includes the equilibrium contribution from the conduction electrons, equal

to $-\alpha_{sd}\bar{m}/|M|$, where $\bar{m}$ is the equilibrium (in the absence of current) magnetization of free electrons.

In (1) and (3), the terms with the coefficient K describe the effect of the torsional moment leading to the transfer of spin from the electrons to the lattice, and the terms with the coefficient P_{sd} describe the effect of the spin-injection mechanism. Equations (1) and (3) can be linearized near the stationary state $\mathbf{M} = (0, 0, \bar{M}_z)$ and $\mathbf{L} = (0, \bar{L}_y, 0)$ to find small oscillations [4]

$$M_x, M_y, \tilde{M}_z = M_z - \bar{M}_z; \quad L_x, \tilde{L}_y = L_y - \bar{L}_y, L_z. \tag{4}$$

The following expressions for stationary solutions can be found from the equations:

$$\bar{M}_z = \frac{H_z + P_{sd}/\gamma}{\Lambda + (\beta - \beta')/2} \approx \frac{H_z + P_{sd}/\gamma}{\Lambda} \tag{5}$$

$$\bar{L}_z = \pm\sqrt{4M_0^2 - \bar{M}_z^2} \approx \pm 2M_0. \tag{6}$$

Note the appearance of an additive to the external magnetizing field created by the parameter P_{sd} that represents the spin injection. This additive describes the effective magnetic field parallel to the injector magnetization and created by the spins of the conduction electrons. It turns out that the beveled configuration of AFM can be obtained without the participation of an external magnetic field.

Thus, the analysis of (1), (2), and (5) shows that the induced magnetic field in AFM under the action of spin-polarized current is also possible in the absence of an external magnetic field H_z. This induced field is proportional to the current density j and the degree of its spin polarization, which, in this case, is determined by the polarization of conductivity Q. However, another quantity characterizing the spin polarization of the flux will be used in the following: $\bar{P} = (n_\downarrow - n_\uparrow)/(n_\downarrow + n_\uparrow)$ is the equilibrium spin polarization. In zero approximation, when $\mu_\downarrow \approx \mu_\uparrow$, what is acceptable according to [23], $\bar{P} \approx Q$, that is, the transition from Q to P is valid.

Thus, under the influence of spin-polarized current, the AFM layer (working area) turns into a magnet with magnetic properties different from those of the injector (FM layer) [26]. The transformation of the FM–AFM junction into a magnetic junction of the FM–FM type allows us to further use the previously obtained results of research on the formation of THz radiation in the FM–FM junction [17], [28]. According to these results, when a spin-balanced current estimated by the equilibrium spin polarization parameter $\bar{P}_1$ passes from the injector to a working area with different magnetic properties and a different value $\bar{P}_2$, energetically excited, spin-unbalanced conduction electrons arise in the latter, determined by the ratio $P = \bar{P}_2 + \Delta P$, where P is the non-equilibrium spin polarization [28], ΔP is the deviation of spin polarization from the equilibrium value in the working area $\bar{P}_2$, and it reaches its highest value at the magnetic layers' boundary. The non-equilibrium additive ΔP can be found from the equation for non-equilibrium spin polarization [29]. In the stationary and quasi-classical approximations and taking into account the difference in the mobility of electrons with different spin projections, this equation has the form

$$\frac{d^2P}{dx^2}\{b(1+b) + (1-b)P)\} - \frac{dP}{dx}\frac{j}{j_D l}b - \left(\frac{dP}{dx}\right)^2 b(1-b^2) - \frac{(P-P_2)}{2l^2}(1+b)^2 - (1-b^2)\frac{(P^2 - P_2P)}{l^2} - (1-b)^2\frac{(P^3 - P_2P^2)}{l^2} = 0 \tag{7}$$

where $b = \mu_+/\mu_-$ is the mobility ratio of electrons with opposite spin directions, $l = \sqrt{D_+\tau}$ is the spin relaxation length for electrons with spin in the magnetization direction, $j_D = e\,n\,D_+/l$ is the current density coinciding in order of magnitude with the diffusion current density at $D_- = D_+ = D$ [29], and $n = n_\downarrow + n_\uparrow$ is the total concentration of electrons in the metal. In the working area of the magnetic junction, the energy change of spin-energy subbands occurs faster than the spin state changes, which leads to the formation in each of the subbands of quasi-Fermi levels $\varepsilon_\downarrow$ and $\varepsilon_\uparrow$, shifted relative to the equilibrium Fermi level ε_F by values determined by the relations [24]

$$\Delta\varepsilon_\downarrow = \varepsilon_\downarrow - (\varepsilon_F - eV/2) \tag{8}$$

$$\Delta\varepsilon_\uparrow = (\varepsilon_F - eV/2) - \varepsilon_\uparrow \tag{9}$$

where V is the potential difference applied to the magnetic junction. It is convenient to express the quasi-Fermi levels defined by (7) and (8) in terms of the equilibrium value P_2 and the non-equilibrium addition ΔP determined by (7) [24]

$$\Delta\varepsilon_\uparrow = \frac{\hbar^2}{2m}(3\pi^2 n)^{2/3}\left|\left(\frac{1-P_2-\Delta P}{2}\right)^{2/3} - \left(\frac{1-P_2}{2}\right)^{2/3}\right| \tag{10}$$

$$\Delta\varepsilon_\downarrow = \frac{\hbar^2}{2m}(3\pi^2 n)^{2/3}\left|\left(\frac{1+P_2}{2}\right)^{2/3} - \left(\frac{1+P_2+\Delta P}{2}\right)^{2/3}\right| \tag{11}$$

where $\hbar$ is the reduced Planck constant and m is the mass of the electron. In (10) and (11), the sign of changes in the quasi-levels depends on the sign of the non-equilibrium spin additive and can be either positive or negative.

The resulting spin-unbalanced energy-excited electrons are able to perform spin-flip transitions with the emission of a quantum of energy, the maximum frequency of which is determined using (10) and (11)

$$\nu = \frac{\Delta\varepsilon_\downarrow + \Delta\varepsilon_\uparrow}{2\pi\hbar} = \frac{|\varepsilon_\downarrow - \varepsilon_F| + |\varepsilon_F - \varepsilon_\uparrow|}{2\pi\hbar} = \frac{\varepsilon_\downarrow - \varepsilon_\uparrow}{2\pi\hbar}. \tag{12}$$

Taking into account the fact that the frequency $\nu > 0$, modulus signs are introduced in (11). The calculation of the frequencies of spin-injection radiation according to (7)–(11) showed that, at a certain current density above the threshold value, these frequencies lie in the terahertz range. It was found that, for the same frequency range, even at small values of the difference in mobility of electrons with spin up and down, the current density can be two orders of magnitude lower than the current density at the same mobility. This allowed us to explain the significant difference (about two orders of magnitude) in the current densities, corresponding

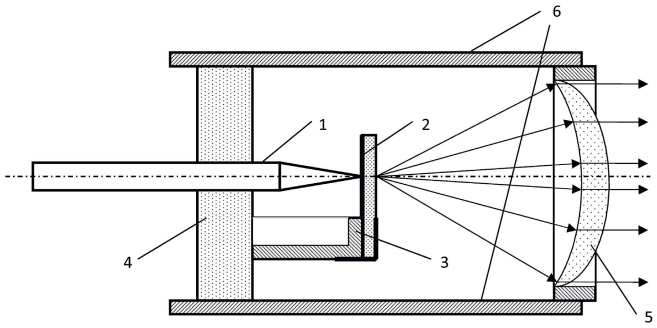

Fig. 2. Spin-injection emitter with a "rod-film" structure. 1—FM rod (steel) with a 10–50 μm sharpness; 2—30 nm-thick FeMn film on a dielectric substrate; 3—substrate holder; 4—dielectric base platform of the emitter; 5—meniscus focusing lens; and 6—lens holder. Thin arrows indicate the flow of radiation.

to the terahertz frequency range, between the theoretical estimate that we made earlier [28] and the measurements in the experiment [18].

The total power of radiation can be determined by knowing the probability of interband radiative quantum transitions R_{st} determined by equation [17]

$$R_{\text{st}} = \frac{6\pi^2 e^2 \mu}{n_{\text{med}}^2 \omega} \frac{(n_\uparrow - n_\downarrow)}{\hbar \nu_s} N_p \left(\frac{\partial I}{\partial p}\right)^2 \left(\cos^2\varphi + \sin^2\varphi \cos^2\theta \sin^2\theta\right) \tag{13}$$

corresponding to the practically significant case $|\partial I/\partial p| p_{F\uparrow} < \hbar\nu_s$ under consideration. Here, I is the exchange interaction energy, p is the electron momentum, $p_{F\uparrow}$ is the Fermi momentum in the energy-excited subband, ν_s is the spin relaxation frequency, μ and n_{med} are the permeability and refractive index of the medium, respectively, N_p is the photon density of the external magnetic field, φ is the angle between the magnetization vectors of the magnetic layers along the Z-axis, and θ is the angle between the magnetization vectors in the XY plane. Thus, taking into account (11), the total radiation power will be defined as $W = 2\pi R_{\text{st}} \hbar\nu$.

III. Experiments

The main goal of the experiments was to confirm the possibility of excitation of intrinsic magnetization in an AFM under the action of a spin-polarized current due to the sd-exchange interaction of the conduction electrons spins with the d electrons of the crystal lattice. The authors also had the task to show the possibility of practical use of AFM in the spin-injection THz range emitters.

The experiments were carried out with two types of emitters. In the first one, a "rod-film" type structure was used [30]. The second used a metabridge (metatransition) type structure [31].

The scheme of the emitter with the "rod-film" structure is shown in Fig. 2. It looks like experiments with point contacts [32] but has a number of significant differences. Thus, if, in the first case, a copper rod with a tip of tens of nanometers is used and the required density of current penetrating several layers of magnetic transition is provided by the nanometer size of the rod tip, in our case, a magnetic rod made of ordinary structural steel is used. It was a cylinder 1.5 mm in diameter and 40 mm long, one end of which was mechanically sharpened, with subsequent grinding of the tip. The diameter of the tip of the rod (regardless of its material) was $\sim$30 μm. It was controlled visually after each measurement cycle using an optical microscope. The current exiting the rod propagates along a film of nanoscale thickness Δ deposited on a dielectric substrate toward a massive collector that contacts the film and is 1 mm away from the rod. The required current density of more than 10^5 A/cm^2 is achieved in the film along the edge of the rod tip due to the nanoscale thickness of the film (conductive section $S = 2\pi r \Delta$). Thus, with a tip diameter of 30 μm and a film thickness of 30 nm, the required current density is achieved at a current of 3 mA. The FM steel rod 1 and the substrate holder 3 functioned as current-carrying electrodes. A film, made of FeMn AFM, applied on a dielectric substrate by epitaxial growth in a vacuum, was used in the experiments. Interestingly, the experiments carried out with a copper rod showed significantly different results from those with a steel rod (see Appendix A). When the voltage was applied to the electrodes, a spin-polarized current, injected from the rod, flowed through the magnetic junction formed by the "rod-film" contact. In general, the change in polarity affects which layer is the injector and which layer is the working region, i.e., it determines the value of equilibrium spin polarization in (7). Nevertheless, in the experiments, the change in the polarity of the current did not have a significant effect on the power and, therefore, is no longer considered in the article. The magnetization of the steel rod is directed along its axis. The spins injected from it are oriented along with the rod magnetization and retain it in the film up to the rod boundary since the direction of the film magnetization under the rod is determined by the rod magnetization. Beyond the rod boundary, the film's magnetization changes, which provides sd-exchange interaction over the spin relaxation length. When the threshold value of the current flowing through the junction (and, accordingly, the current density in the magnetic junction) was exceeded, electromagnetic radiation of the THz range was excited in it. The excitation of radiation leads to a violation of the monotonicity of the increase in the resistance with increasing current (voltage) and the appearance of negative differential resistance (see Appendix B). The radiation (shown in Fig. 2 by thin arrows), generated at the "rod-film" contact point, was almost evenly spherically distributed around the magnetic junction. Part of the concentrically emitted signal fell on the focusing lens, converting it into a paraxial beam. The power it carried was registered by the opto-acoustic detector (Golay cell). It should be emphasized that we are considering radiation from the film region limited by the diameter of the rod and the distance from it equal to the spin relaxation length. It is in this region that the maximum current density is reached, determined by the relation $S = 2\pi r \Delta$, where r is the radius of the rod tip and Δ is the film thickness. In this particular case, the injector and the work area are located in the thickness of a single film. The spin state of the electron flow is disrupted by changing the direction of the film's magnetization, which is determined by the rod's magnetization [33]. As for the influence of cleanliness of contacting surfaces, their

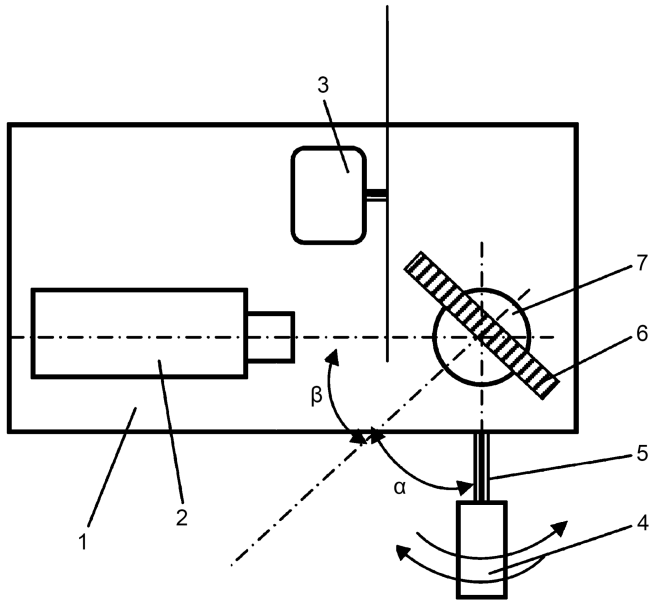

Fig. 3. Scheme of the experimental setup for studying frequency characteristics using a diffraction grating. Number 1 indicates the platform on which the Goley cell 2 (signal detector) and the THz signal modulator (chopper) 3 are installed. The spin-injection emitter 4 is fixed on a rotating bench 5 that rotates in the plane of the platform relative to the surface of the diffraction grating 6. It is mounted on rotating table 7 so that the grating surface is perpendicular to the surface of the platform. Angle α is the angle of incidence of the signal on the diffraction grating, and angle β is the angle of registration of one of the diffraction harmonics of the signal, which is set by means of the rotating table 7 before the measurements.

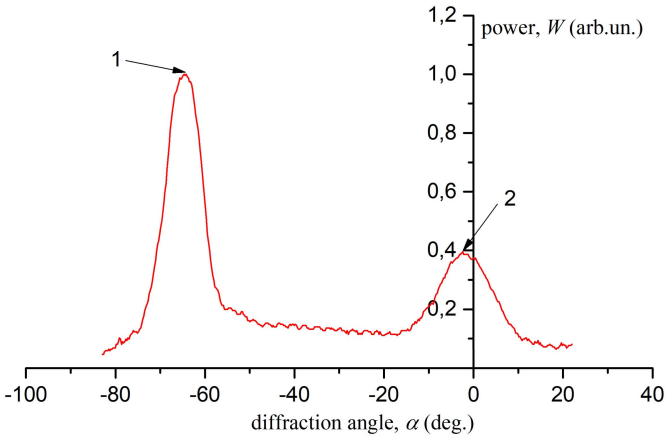

Fig. 4. Region of the angular diffraction spectrum measured with a diffraction grating for $I = 220$ mA.

"contamination" can lead to a decrease in the conductive surface and, as a consequence, increase the current density under the rod [34].

During the operation of the emitter, an external magnetic field is not required since the radiation is formed due to the intrinsic magnetization of the contacting layers. However, since the rod was partially demagnetized over time, it was periodically magnetized by an external magnetic field up to 1.5 T for about a minute, placing it between the tips of the electromagnet perpendicular to their surface. This led to an increase in the efficiency of the emitter up to 20%.

The radiation frequency was evaluated using a diffraction grating according to the method described in [35]. The scheme of the measuring setup for such an evaluation is shown in Fig. 3. The technique of determining the wavelength of the radiated THz signal is based on the effect of diffraction radiation when, at the fall of the electromagnetic wave with a length λ, comparable to the period of the lattice l, the wave diffraction occurs. In this case, the angle of wave incidence α is related to the angle of reflection β by the ratio

$$\sin\alpha - \sin\beta = n\lambda/l. \tag{14}$$

In (13), the parameter n is the number of the spatial harmonic, which can take both positive and negative integer values. The angles α and β were counted from the normal to the diffraction grating surface. At the same time, the angle β in a particular measurement was fixed with a certain value, and the angle α changed in the range from $\alpha = -\beta$ to $\alpha = 90°$. At some value of angle α, the first diffraction peak from the "zero" harmonic was registered. Thus, knowing the angle β, the period of the diffraction lattice l, the number of the diffraction harmonic $n = 1$, and determining the angle α, at which the first diffraction peak from the "zero" harmonic is observed, the wavelength of the radiated THz signal was determined by (13). Fig. 4 shows the spectrum of diffraction harmonics measured at 220 mA. Here, number 1 indicates the diffraction peak of the zero harmonic; corresponding to the angle β, number 2 indicates the diffraction peak of the first harmonic, observed at the angle α. The width of the diffraction peaks (zero and first) due to their diffraction blurring is determined by the measurement resolution. Nevertheless, the frequency of the emitted signal can be estimated from the maximum of the first harmonic.

According to this method, the central frequency of radiation was estimated at $\nu = 16$ THz. This radiation is formed due to the appearance of intrinsic magnetization in the AFM under the action of the polarized current, which is determined, as in the case of the FMs, by the equilibrium spin polarization. Furthermore, to establish the identity of the registered signal of the emitter using FeMn AFM film with the signals of emitters using FM films Fe, Co, and Ni [36], we use the connection of the radiated frequency ν with the equilibrium spin polarization of the magnet $\bar{P}$. This relationship follows from (11), taking into account (10) and (11). In general, we do not know the value of equilibrium spin polarization $\bar{P}$ for FeMn. However, it can be estimated from the experimentally measured radiation frequency. For this purpose, let us compare the signal of the emitter using the AFM FeMn film with the signals of the emitters using Fe, Co, and Ni FM films [36] with known values of equilibrium spin polarization. Fig. 5 shows the relationship between the radiation frequency ν and the value $\bar{P}$ for Ni, Co, and Fe films. Taking into account the linear dependence of ν on $\bar{P}$ for Fe, Co, and Ni and extrapolating it (in Fig. 5, a thin solid line), we estimate the $\bar{P}$ value for the FeMn film from the experimentally measured frequency. From Fig. 5, it can be seen that its value is $\bar{P} \sim 0.45$. In general, the results presented in Fig. 5 show the identity of the recorded signals using different films, including the AFM FeMn film.

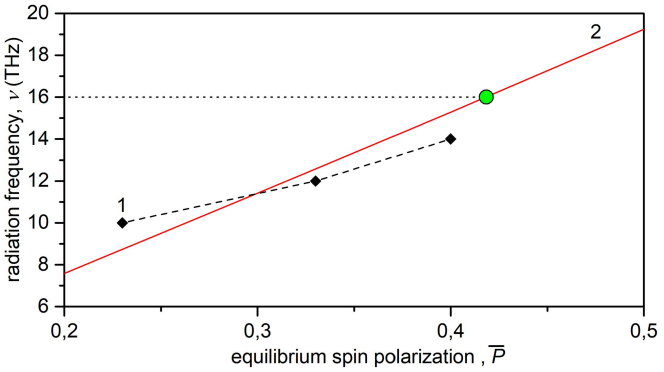

Fig. 5. Dependence of the radiation frequency ν on the value of the equilibrium spin polarization $\bar{P}$ of the working layer. Curve 1 corresponds to the experimentally measured frequencies for the working layers of Ni ($\bar{P} = 0.23$), Co ($\bar{P} = 0.33$), and Fe ($\bar{P} = 0.4$), and curve 2 corresponds to the calculated frequency values. The heavy dot on curve 2 corresponds to the case of using the FeMn film.

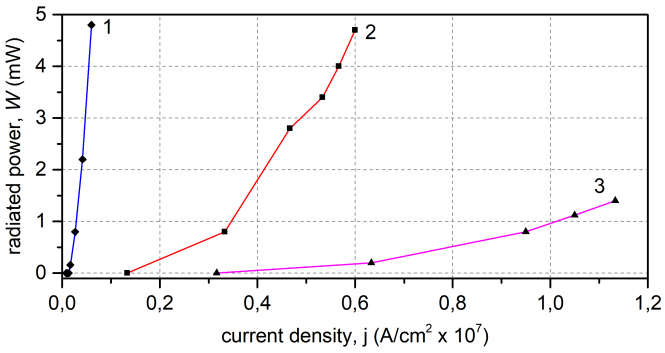

Fig. 6. Dependence of the radiated power W on the current density j flowing through the magnetic transition for the emitter structure with different films: 1—Fe_3O_4; 2—FeMn; and 3—Fe.

Having estimated the value of the equilibrium spin polarization for the AFM film $\bar{P} \sim 0.45$, we estimate the radiation frequency by formula (11), taking into account (10) and (11). To do this, we take $P_2 \sim 0.45$ and $P_1 \sim 0.4$ (steel rod). In addition, we assume in (10) that $\varphi = 180^0$ and $j/j_D = 0.1$, taking into account the difference in the mobility of electrons with different spins. Then, $\Delta P = 0.085$. According to (11), after substituting the universal constants and obtained values, we have $\Delta\varepsilon_\uparrow = 1.3 \cdot 10^{-20}$ and $\Delta\varepsilon_\downarrow = 0.96 \cdot 10^{-20}$. Substituting these values in (11), we determine the frequency $\nu = 36.3$ THz. Its comparison with the experimentally measured frequency $\nu = 16.5$ THz shows a quite acceptable correspondence.

Thus, it is shown that, under the action of spin-polarized current, AFM becomes a magnetic with its own value of equilibrium spin polarization $\bar{P}$. In the framework of our representations, the power of spin-injection radiation, according to (13), depends mainly on the value $\bar{P}$ (the power of radiation W is proportional to $n\uparrow - n\downarrow = n\bar{P}$, where n is the total concentration of free charges in metal). The higher the value $\bar{P}$, the higher the efficiency of the emitter (lower starting current value and greater radiation power at equal current values). The results of the energy efficiency study of emitters with different magnetic films (Fe_3O_4, FeMn, and Fe) are presented in Fig. 6. Here, on the vertical axis, the integral radiation power calculated taking into account its uniform scattering from the point of contact into the 4π sphere is presented. They confirm the dependence of the power of the emitted signal on the value $\bar{P}$ of the magnetic film used. This can be seen from the comparison of the dependence of radiation power on current for two films with known values $\bar{P}$-Fe_3O_4 ($\bar{P} \sim 1$) and Fe ($\bar{P} \sim 0.4$). For FeMn, the starting and operating currents are higher than for Fe_3O_4 film but lower than for Fe film. This is in line with the earlier assumption that the value $\bar{P}$ for FeMn is slightly higher than for Fe.

When comparing the radiation power of different films, it should be borne in mind that the registered signal is only a part of the power emitted during spin-flip transitions since a certain number of radiated quanta is absorbed in the thickness of the film. In our opinion, this absorption is related to the skin layer, so the thickness of the magnetic films used should not exceed its size. In this work, the emphasis was placed only on the dependence of the radiation power on the value $\bar{P}$; therefore, in experiments, films with close values of thickness not exceeding the thickness of the skin layer were used. Here, as above, the current density was determined by the formula $j = I/S$. The nature of the dependence of the radiation power on the current density is close to the quadratic, which follows from (13), which determines the number of quantum transitions R_{st} when substituting the value of non-equilibrium spin polarization $P = \overline{P}_2 + \Delta P$ into it, where ΔP is defined by (7). In general, the results presented in Fig. 6 indirectly confirm the transition of the AFM FeMn to a magnetic with its own equilibrium spin polarization $\bar{P}$ under the action of spin-polarized current.

The above results relate to the study of a single magnetic transition. From the point of view of increasing the radiation power of a spin-injection emitter, an emitter whose structure is formed by many magnetic transitions is of interest. As one of the variants of such an emitter, we considered an emitter of the metatransition type, as described in detail in [31] and [37]. Its structure is shown in Fig. 7. In it, non-percolated Fe rods 15–20 nm high and 50–70 nm in diameter, spaced 10–15 nm apart, are deposited on a dielectric substrate with a thickness of 500 μm and coated on top with a FeMn AFM with a thickness up to $\Delta \sim 30$ nm. Current-carrying contact pads, made particularly from Mo, are provided to supply voltage to the transition. The distance between contact pads $L = 100$ μm, and the width of metatransition $D = 200$ μm. Fig. 8 shows the granular structure of the metatransition formed by electrically unbound Fe islands, taken with a scanning probe microscope. Subsequently, the islands are covered by a continuous nanometer-thick FeMn layer so that FeMn fills the space between the islands, binding them electrically.

Since the FeMn resistivity is much higher than that of Fe, the current flowing between the contact pads in the structure under consideration seemed to be "focused" in the iron rods, which, in our opinion, significantly increased its density in each of the FeMn–Fe contacts along the rod boundary.

The fact that the resistance of the rods is almost an order of magnitude lower than that of the FeMn layer, along with

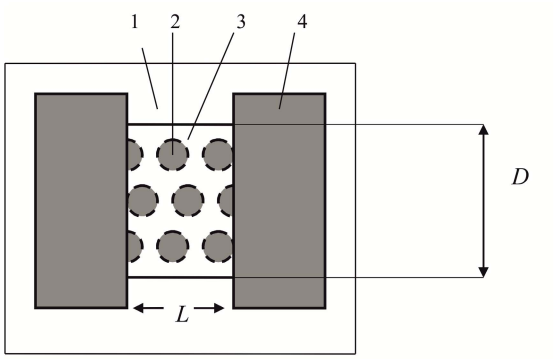

Fig. 7. Metatransition-based emitter (top view): 1—dielectric substrate; 2—iron rods; 3—AFM metal FeMn layer covering the iron rods of nanoscale thickness; 4—current-carrying contact pads, and L and D—dimensions of the metatransition.

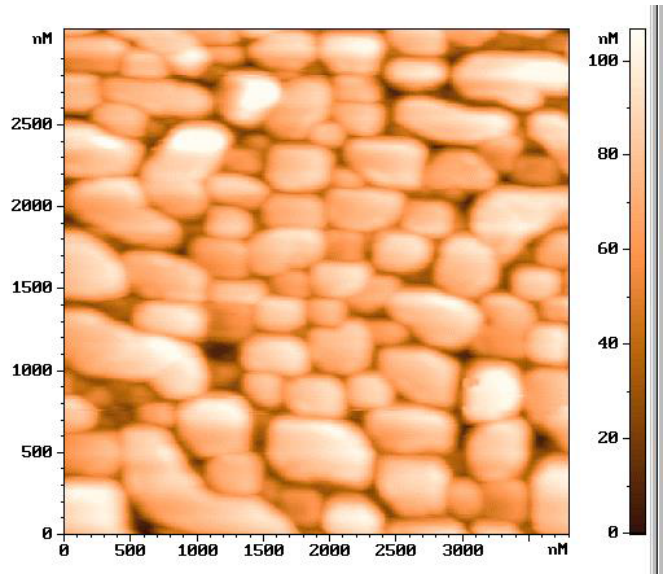

Fig. 8. Microscopic structure of one of the metatransition samples.

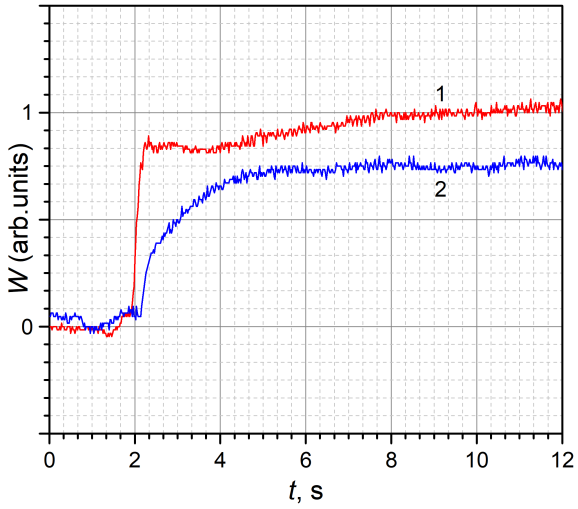

Fig. 9. Oscillograms of power rise of emitter output signal in arbitrary (relative) units when the emitter with the metatransition (with Fe rods) structure (curve 1) and the emitter without Fe rods structure (curve 2) are turned on.

the small geometric dimensions of the transitions themselves, provided the necessary current density in the transitions at the boundary of each of the rods for the mini-emitter to operate at currents of the same order as the currents registered in experiments with the "rod-film" emitter structure.

The frequency range (7–30 THz) of spin-injection radiation studied in the work is close to the maximum of Planck's curve of the spectral density of thermal radiation of physical bodies. The possible presence of intense thermal radiation from the heated surface of the emitter raises doubts: does the radiation observed in THz experiments have a magnetic nature? Perhaps, the easiest way to determine the nature of radiation is to determine the rate of rise of the signal when the current is turned on. Thus, if, for thermal radiation, the time of setting the radiation mode is 3–5 s, for spin-injection radiation, the time of establishing interband transitions of electrons, forming the radiation, is 10^{-13} s. In the experiment, the time of setting the spin-injection radiation mode is determined by the inertia of the measuring equipment that we use (~100 ms). This leads to a difference in the rising fronts of the signal when the current is turned on in different structures.

In order to determine the non-thermal nature of the radiation observed in the emitter with metatransition, oscillograms of the power rise front of the emitted signal (after applying voltage) for the above-considered structure of the emitter with Fe rods and the structure without rods were analyzed. Fig. 9 (curve 1) shows an oscillogram for the emitter with Fe rods covered by a film of FeMn AFMs. In this case, it can be seen that the leading edge has a jump-like appearance since the time of spin-flip transitions is ~10–13 s. However, the leading edge has a certain rise time interval of ~90 ms, determined by the inertia of the measuring equipment. For comparison with thermal radiation, Fig. 9 shows an oscillogram (curve 2), corresponding to the emitter with a FeMn AFM film without Fe rods, when the transition was a continuous FeMn film, without any inclusions. For such an emitter, there is a smoother increase in signal power within 4–5 s, which is typical for thermal radiation. The comparison of the two operating modes is based on the following. According to the Rayleigh–Jeans law, thermal radiation is proportional to the area of the radiating surface and its temperature. Thus, if the areas are equal (in our case, $S = 100 \times 200\ \mu\text{m}^2$), the character of changes in the radiation power is adequate to the character of changes in the body temperature. The change in the body temperature from an internal source is determined by the power of the internal heater and the emissivity of the body surface. In both experiments, the radiating surface area is the same, and it is the surface of the FeMn AFM film in both cases. Oscillograms were taken at the following parameters: for the metatransition with Fe columns, $I = 197$ mA and $U = 8$ V; for the case without columns, $I = 250$ mA and $U = 6$ V, that is, in both cases, the power released by the current is almost the same. Nevertheless, there is a significant difference in the time of setting the radiation mode—almost two orders of magnitude from the same radiating surfaces. In addition, in curve 1 of

Fig. 9, three areas can be distinguished: the area of jump-like change in power corresponding to current turn-on (first area), then almost a shelf (second area), and the area of smooth increase in power (third area). The first two areas, according to the authors, are of a non-thermal nature. The beginning of the third area in the figure is observed after 3 s. During these 3 s, the body temperature reaches a value that provides thermal radiation power, noticeable against the background of dynamic radiation. On the oscillogram, this is the area of smooth power increase. Curve 2 in Fig. 9, corresponding to thermal radiation, has only a smooth character of power increase after switching ON.

Evaluation of the signal frequencies of the highest intensity using the diffraction grating showed the difference in their values. Thus, for the transition without Fe columns, the frequency was 12.5 THz, and for the metatransition with Fe columns, the frequency was 8.4 THz. A more detailed study of the spectra in these measurements was not carried out.

The magnetic nature of spin-injection radiation should also be manifested in the dependence of the radiation power on the influence of an external magnetic field. Thus, according to (13), the radiation power is directly proportional to $\cos^2\varphi$, that is, it depends on the angle between the magnetization vectors of the magnetic transition layers. It takes the highest value when $\varphi = 0$ or π. In general, the orientation of the magnetization of iron rods in the metatransition is arbitrary and takes values in the range $\varphi = 0 \div \pi$. Under the action of an external magnetic field, the magnetization of various rods is ordered, being oriented along the vector of the external magnetic field, and φ takes the value 0 or π, which increases the radiation power.

To prove the magnetic nature of the observed radiation, Fig. 10 shows the experimental results of measuring the dependence of the radiation power on the power consumed by the emitter ($W_{\text{cons.}} = U \cdot I$), demonstrating the effect of the external magnetic field of 1.5 T on metatransition. The ordering of the magnetization of the rods was arranged by placing the sample between the tips of the electromagnet in a plane along the vector of magnetic field 1.5 T just before the work of the emitter. During the operation of the emitter, there was no external magnetic field. The impact occurred for 60 s just before the voltage was applied to the transition. After that, the emitter functioned as usual. In this picture, curve 1 corresponds to the case after such impact, and curve 2 corresponds to the case before impact. There was no external magnetic field during the operation of the emitter. It can be seen from Fig. 10 that the radiation power of the same source, which consumes the same power from an external source, almost doubles after exposure of the emitter to an external magnetic field (compare curves 1 and 2 in Fig. 10). The significant increase in the emitter's energy efficiency after exposure to an external magnetic field (curve 1) seems to be explained by the new, higher degree of order of the metatransition's magnetic structure. In any case, this rather unexpected result requires further research.

For comparison of different emitter designs, a similar dependence is presented for the emitter with a "rod-film" structure (curve 3). Here, it is clear that the emitter with metatransition has many times greater energy efficiency. This is explained by the fact that, when currents of similar magnitude (current densities) occur in magnetic transitions, radiation in the "rod-film" structure is observed only at a distance of the spin relaxation length $l \sim 30$ nm from the edge of the tip of one rod used. In the case of a metatransition, radiation processes can occur along its entire surface (with a large number of "rod-film" magnetic transitions), at least where conditions for the inverse population of spin energy subbands are preserved.

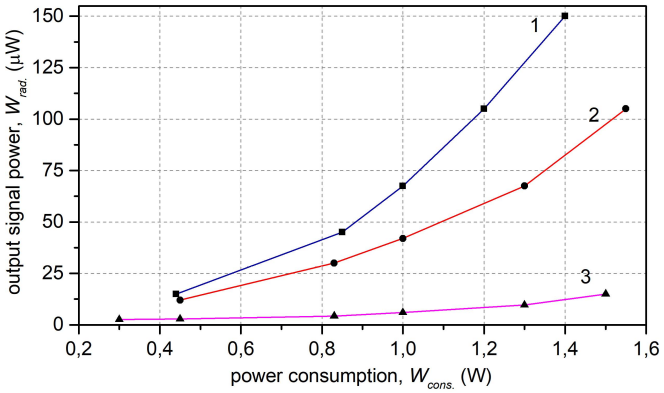

Fig. 10. Dependence of the output signal power $W_{\text{rad.}}$ of the emitter from its power consumption $W_{\text{cons.}}$. 1—Emitter with metatransition after exposure to the external magnetic field; 2—emitter with metatransition before exposure to the external magnetic field; and 3—emitter with the "rod-film" structure.

IV. Conclusion

The original method of the intrinsic magnetization excitation in the AFM layer of the FM–AFM magnetic nanojunction is considered. It is determined by sublattices beveling of the AFM layer with a relatively small spin-polarized current (tens of mA) flowing through the junction. The resulting intrinsic magnetization of the AFM interacts with the spin-polarized current, which leads to the appearance of spin-unbalanced electrons and, as a result, to the excitation of electromagnetic oscillations of the THz range. Experimental results showing the efficiency of the considered method by the example of using FeMn AFM film in magnetic junctions of THz emitters of different structures are presented. In addition, it has been experimentally shown that the use of the AFM layer provides additional opportunities to reduce starting currents and change the frequency of radiation.

Appendix A
Effect of Rod Material on Radiation

In the rod-film structure using the FeMn film, the rod material determines the possibility of the formation of a magnetic transition at the contact point and, as a consequence, the occurrence of spin-injected THz radiation. In order to investigate the various radiative processes occurring in the structure under study when current flows, experiments were conducted using a steel rod, which formed a magnetic transition and a copper rod, in the presence of which no magnetic transition was formed. To control the identity of the measurements performed, after each measurement of the dynamic parameters presented in

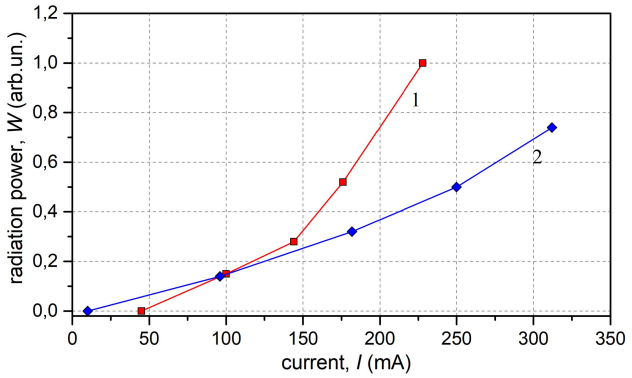

Fig. 11. Dependence of radiation power on current when using FeMn film for steel (curve 1) and copper (curve 2) rods.

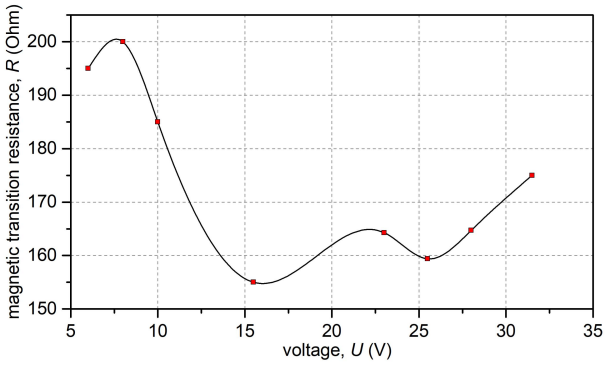

Fig. 12. Dependence of the magnetic transition resistance R on the voltage U applied to it.

Fig. 11, the diameter of the sharpening of the rods, both copper and steel, was checked visually with an optical microscope. The tip diameters were about 30 μm within a measurement error of 5%. From the point of view of thermal radiation, the difference in the structures of the emitters consists only of more efficient heat removal from the contact area of the film with the copper rod and its less heating by the Joule heat, i.e., at a lower temperature of the structure. According to Rayleigh–Jeans' law, the power of thermal radiation is proportional to the area of the radiating surface and its temperature. Thus, if only thermal radiation is observed in both cases, then the dependencies of the radiated power on the current of the studied structures should not intersect since only their temperatures are different. With a heated surface area of a few square centimeters, which, in our case, is heated within a few seconds (see the smooth rise of the amplitude in Fig. 9), the power of thermal radiation can reach significant values and can be easily recorded. However, the results shown in Fig. 11 are somewhat unusual in terms of thermal radiation. Thus, assuming only the thermal nature of the radiation, one would expect a lower "starting current" when using a steel rod than when using a copper rod. However, we see the opposite situation. The presence of a magnetic transition seems to "slow down" the thermal radiation. Therefore, it is unlikely that, when using a steel rod, the radiation can only be associated with heat. This phenomenon is currently being intensively studied by us, and a publication is being prepared based on the research results.

Appendix B
Dependence of the Magnetic Transition Resistance on Voltage

A typical dependence of the resistance on the voltage applied to the magnetic transition is shown in Fig. 12. Such an ohmic dependence is typical for an active element, where the section with a negative differential resistance (voltage range: $7 \div 15$ V) indicates, in our opinion, the excitation of electromagnetic oscillations in it. Under the influence of the current, the structure of the transmitter heats up, which leads to an increase in its total resistance. Starting from a certain voltage value (corresponds to 15 V on the graph), the thermal addition to the resistance prevails over the negative addition, which leads to an increase in the total resistance of the emitter structure. At the same time, the dynamic radiation is preserved.

Acknowledgment

This work was supported in part by the Russian Foundation for Basic Research under Grant 20-07-00349 A and within the state assignment of the Kotel'nikov Institute of Radio Engineering and Electronics of the Russian Academy of Sciences (RAS).

References

[1] T. Jungwirth, X. Marti, P. Wadley, and J. Wunderlich, "Antiferromagnetic spintronics," *Nature Nanotechnol.*, vol. 11, no. 3, pp. 231–241, Mar. 2016.
[2] S. S. Dhillon *et al.*, "The 2017 terahertz science and technology roadmap," *J. Phys. D, Appl. Phys.*, vol. 50, no. 4, Feb. 2017, Art. no. 043001.
[3] F. Hellman *et al.*, "Interface-induced phenomena in magnetism," *Rev. Mod. Phys.*, vol. 89, no. 2, Jun. 2017, Art. no. 025006.
[4] Y. V. Gulyaev, P. E. Zil'berman, and S. G. Chigarev, "Spin-injection generators of terahertz waves based on metal magnetic structures," *J. Commun. Technol. Electron.*, vol. 60, no. 5, pp. 411–435, May 2015.
[5] A. Kadigrobov, Z. Ivanov, T. Claeson, R. I. Shekhter, and M. Jonson, "Giant lasing effect in magnetic nanoconductors," *Europhys. Lett. EPL*, vol. 67, no. 6, pp. 948–954, Sep. 2004.
[6] R. Khymyn, I. Lisenkov, V. Tiberkevich, B. A. Ivanov, and A. Slavin, "Antiferromagnetic THz-frequency Josephson-like oscillator driven by spin current," *Sci. Rep.*, vol. 7, no. 1, Mar. 2017, Art. no. 43705.
[7] O. R. Sulymenko, O. V. Prokopenko, V. S. Tiberkevich, A. N. Slavin, B. A. Ivanov, and R. S. Khymyn, "Terahertz-frequency spin Hall auto-oscillator based on a canted antiferromagnet," *Phys. Rev. A, Gen. Phys.*, vol. 8, no. 6, Dec. 2017, Art. no. 064007.
[8] A. M. Kadigrobov, R. I. Shekhter, and M. Jonson, "Photon generation in ferromagnetic point contacts," *Low Temp. Phys.*, vol. 38, no. 12, pp. 1133–1138, Dec. 2012.
[9] S. Urazhdin and N. Anthony, "Effect of polarized current on the magnetic state of an antiferromagnet," *Phys. Rev. Lett.*, vol. 99, no. 4, Jul. 2007, Art. no. 046602.
[10] E. V. Gomonai and V. M. Loktev, "Distinctive effects of a spin-polarized current on the static and dynamic properties of an antiferromagnetic conductor," *Low Temp. Phys.*, vol. 34, no. 3, pp. 198–206, Mar. 2008.
[11] H. Gomonay and V. Loktev, "Spin-polarized current-induced instability in the spin-valve antiferromagnetic layer," *J. Magn. Soc. Jpn.*, vol. 32, no. 6, pp. 535–539, 2008.
[12] A. S. Núñez, R. A. Duine, P. Haney, and A. H. MacDonald, "Theory of spin torques and giant magnetoresistance in antiferromagnetic metals," *Phys. Rev. B, Condens. Matter*, vol. 73, no. 21, Jun. 2006, Art. no. 214426.
[13] Z. Wei *et al.*, "Changing exchange bias in spin valves with an electric current," *Phys. Rev. Lett.*, vol. 98, no. 11, Mar. 2007, Art. no. 116603.

[14] Z. Wei, A. Sharma, J. Bass, and M. Tsoi, "Point-contact search for antiferromagnetic giant magnetoresistance," *J. Appl. Phys.*, vol. 105, no. 7, Apr. 2009, Art. no. 07D113.
[15] J. Basset, Z. Wei, and M. Tsoi, "Current-induced reorientation of exchange bias on a nanoscale," *IEEE Trans. Magn.*, vol. 46, no. 6, pp. 1770–1772, Jun. 2010.
[16] Y. V. Gulyaev, P. E. Zil'berman, A. I. Krikunov, A. I. Panas, and É. M. Éphshteĭn, "Current-induced inverse population of spin subbands in magnetic junctions," *JETP Lett.*, vol. 85, no. 3, pp. 160–164, Apr. 2007.
[17] Y. V. Gulyaev, E. A. Vilkov, P. E. Zil'berman, G. M. Mikhailov, and S. G. Chigarev, "Sd-exchange emission in ferromagnetic junctions," *J. Commun. Technol. Electron.*, vol. 58, no. 12, pp. 1137–1141, Dec. 2013.
[18] Y. V. Gulyaev *et al.*, "Spin-injection terahertz radiation in magnetic junctions," *JETP Lett.*, vol. 93, no. 5, pp. 259–262, May 2011.
[19] V. Yu Gulyaev, E. A. Vilkov, P. E. Zil'berman, G. M. Mikhailov, A. V. Chernykh, and S. G. Chigarev, "Stimulated terahertz emission," *J. Commun. Technol. Electron.*, vol. 60, no. 9, pp. 1016–1019, Sep. 2015.
[20] A. G. Aronov and G. E. Pikus, "Spin injection into semiconductors," *Sov. Phys. Semicond.*, vol. 10, no. 6, pp. 698–700, 1976.
[21] C. Heide, P. E. Zilberman, and R. J. Elliott, "Current-driven switching of magnetic layers," *Phys. Rev. B, Condens. Matter*, vol. 63, no. 6, Jan. 2001, Art. no. 064424.
[22] V. Yu Gulyaev, P. E. Zil'berman, and E. M. Epshtein, "The effect of spin injection on the domain structure and the conductance of a magnetic junction," *J. Commun. Technol. Electron.*, vol. 46, no. 7, pp. 794–801, 2001.
[23] V. Y. Gulyaev, P. E. Zil'berman, E. M. Epshtein, and R. J. Elliott, "Spin injection by current in metal-metal magnetic junctions," *J. Commun. Technol. Electron.*, vol. 48, no. 9, pp. 942–956, 2003.
[24] Y. V. Gulyaev, P. E. Zilberman, and E. M. Epshtein, "Effect of current on magnetization oscillations in the ferromagnet-antiferromagnet junction," *J. Experim. Theor. Phys.*, vol. 114, no. 2, pp. 296–304, Feb. 2012.
[25] Y. V. Gulyaev, P. E. Zilberman, V. D. Kotov, G. M. Mikhailov, S. G. Chigarev, and E. M. Epshtein, "Current-induced resonance in ferromagnet-antiferromagnet junctions," *J. Commun. Technol. Electron.*, vol. 57, no. 8, pp. 813–817, Aug. 2012.
[26] Y. V. Gulayev, P. E. Zil'berman, S. I. Kasatkin, G. M. Mikhailov, and S. G. Chigarev, "Terahertz emission in the ferromagnetic-antiferromagnetic structure," *J. Commun. Technol. Electron.*, vol. 58, no. 7, pp. 716–719, Jul. 2013.
[27] A. I. Akhiezer, V. G. Bar'yakhtar, and S. V. Peletminskii, *Spin Waves*. Amsterdam, The Netherlands: North-Holland, 1968.
[28] E. A. Vilkov *et al.*, "Frequency tuning of the spin-injection radiation in the magnetic contact junction," *J. Commun. Technol. Electron.*, vol. 61, no. 9, pp. 995–1002, Sep. 2016.
[29] E. A. Vilkov, S. A. Nikitov, O. A. Byshevskii-Konopko, A. R. Safin, L. A. Fomin, and S. G. Chigarev, "Frequency of spin-injection radiation in the magnetic junction as a function of the spin mobility of electrons," *Phys. Solid State*, vol. 62, no. 9, pp. 1671–1677, Sep. 2020.
[30] V. Y. Gulyaev, P. E. Zil'berman, A. I. Panas, E. M. Epshtein, and S. G. Chigarev, "Solid-state electromagnetic radiation source," RU Patent 2 464 683 C1, Oct. 20, 2012.
[31] E. A. Vilkov *et al.*, "Solid-state electromagnetic radiation source," RU Patent 2 688 096 C2, May 20, 2019.
[32] Y. Ji, C. L. Chien, and M. D. Stiles, "Current-induced spin-wave excitations in a single ferromagnetic layer," *Phys. Rev. Lett.*, vol. 90, no. 10, Mar. 2003, Art. no. 106601.
[33] E. A. Vilkov, P. E. Zil'berman, S. G. Moiseev, and S. G. Chigarev, "The magnetostatic field in a terahertz rod/film structure," *J. Commun. Technol. Electron.*, vol. 59, no. 11, pp. 1265–1273, Nov. 2014.
[34] E. Vilkov and S. G. Chigarev, "The density of current flowing through a contact of the rod-film magnetic junction of spin-injection generator," *Zhurnal Radioelektroniki J. Radio Electron.*, no. 7, pp. 1–8, Jul. 2017. [Online]. Available: http://jre.cplire.ru/jre/jul17/4/text.pdf
[35] S. G. Chigarev, I. V. Malikov, and G. M. Mikhailov, "Analysis of the frequency characteristics of the spin-injection emitter in the terahertz range using a diffraction grating," *J. Commun. Technol. Electron.*, vol. 58, no. 3, pp. 238–242, Mar. 2013.
[36] R. Meservey and P. M. Tedrow, "Spin-polarized electron tunneling," *Phys. Rep.*, vol. 238, no. 4, pp. 173–243, 1994.
[37] E. A. Vilkov *et al.*, "A spin-injection terahertz generator based on the metatransition monolithic structure," *J. Commun. Technol. Electron.*, vol. 60, no. 9, pp. 1044–1047, Sep. 2015.